

Temperature effect on the nanosecond laser-induced damage of TiO₂ films with two additives

MING MA^a, CHENG XU^{a*}, DI LIN^a, HUANHUAN SUN^a, ENZHU LIN^a, PEIZHONG FENG^a,
YINGHUAI QIANG^a, DAWEI LI^b

^a*School of Materials Science and Engineering, China University of Mining and Technology, Xuzhou 221116, China*

^b*Key Laboratory of High Power Laser Materials, Shanghai Institute of Optics and Fine Mechanics, Chinese Academy of Sciences, Shanghai 201800, China*

TiO₂ films were prepared using a very stable sol with two additives of diethanolamine (DEA) and polyethylene glycol (PEG) and remained intact without carbonization and cracking at high annealing temperature. It was shown that the laser-induced damage threshold (LIDT) at the wavelength of 1064 nm and the effective pulse duration of 12 ns of the films decreased with the annealing temperature increase. Because of the three-dimensional network structure and the low defect density, the annealing temperature of 353 K led to the highest LIDT of 14.3 J/cm². After annealed at 423 K, the ordered film structure was damaged to some extent and the inner defects emerged, contributing to the slight reduce of LIDT. Continually, the increasing annealing temperature of 523 K resulted in the gradual increase of the defect density and surface roughness and the significant decrease of the LIDT. When the annealing temperature increased further to 623 K, the film surface became much rougher, and more defects including the grain boundaries and the holes appeared which caused the lowest LIDT. According to the LIDT results and damage morphologies, a structure evolution model of the films at different temperatures was proposed.

(Received August 5, 2016; accepted April 6, 2017)

Keywords: TiO₂ films, Laser damage, Annealing, Defects

1. Introduction

The laser damage resistance of optical films is one of the key factors to determine the output power of high power laser, and it affects the stability and the service life of the laser system. Therefore, it is of great significance to improve the laser-induced damage threshold (LIDT) of films for the development and application of laser system [1-3]. The films prepared by the sol-gel method always possess a few attractive features such as the low defect density and good surface morphologies [4]. Moreover, the three-dimensional network and porous structure of sol-gel films help alleviate the damage caused by the local expansion of the films under laser radiation. Therefore, most of the sol-gel films tend to obtain higher LIDT than the physical vapor deposition (PVD) films [5-7].

Due to the popular application in aerospace, military and other fields, there is an increasing influence of environmental factors on the laser system. It is necessary to consider the environmental factors especially the effect of high temperature on the films in the laser system. As is known to all, the disadvantage of sol-gel films is the poor high temperature resistance. However, to our best knowledge, few studies have been reported on the influence of high temperature on the LIDT of sol-gel films. Previous researches revealed that the instability of the sol-gel films under high temperature was generally related to the organic additives [8-11]. With the addition of additives such as acetylacetone (ACAC), diethanolamine (DEA), polyethylene glycol (PEG) and polyvinyl pyrrolidone (PVP), a stable sol was obtained before film

preparation. Usually, one of these additives above is used and the films obtained are prone to carbonization and cracking under high temperature. Once this happens, the LIDT of the films will decrease significantly.

The main aim of this study was to investigate the nanosecond LIDT of TiO₂ films with two additives after high temperature annealing. Firstly, TiO₂ sol was synthesized using tetrabutyl titanate (TTIP) as the precursor and DEA and PEG 200 as two additives. Then, TiO₂ films were prepared by the dip coating method. Finally, annealing at different temperatures was performed on these as-deposited films. The optical properties, structures, photoluminescence spectra, surface morphologies, TG-DSC curves, LIDT and damage morphologies of the films were measured and discussed. Moreover, a structure evolution model of the films was proposed based on the LIDT results and damage morphologies.

2. Experimental

For synthesizing TiO₂ sol, TTIP, ethanol, DEA, PEG 200 and water, were mixed with molar ratios of 1:40:0.83:0.17:2. Firstly, TTIP was dissolved in ethanol. Then after vigorous stirring for 20 min at room temperature, DEA, PEG 200 and water were added by drops to the above solution with a burette under stirring, respectively. Finally, the sol was aged at 276 K for 7 days.

Before preparing the films, BK7 substrates were cleaned carefully with ethanol under ultrasonic. The

substrates were dip-coated at 60 mm/min using the TiO_2 sol above, and then the deposited films were heated at 353 K for 6 min. This coating and heating process was repeated until the films reached up to a certain thickness. In this study, annealing at 353 K was directly performed on the as-deposited film in the air for 1 h. With regard to higher temperature annealing, the as-deposited films were firstly annealed at 353 K for 1 h, and then annealed at 423 K, 523 K and 623 K for 1 h in the air, respectively. All the annealed films were colorless and crack-free under optical microscopy.

The viscosity of TiO_2 sol was measured by Glass Capillary Viscometers at 293 K. Transmittance spectra of the films were performed by using a Lambda 900 spectrophotometer in the range of 250-1800 nm. Structures of the films were determined by a D8 Advance X-ray diffractometer (XRD). Photoluminescence spectra were measured by a Cary 3000 fluorescence spectrophotometer with an excitation laser at 310 nm wavelength. Surface morphologies of the films were characterized by a Sirion 200 field emission scanning electron microscope (FESEM) and a Dimension V atomic force microscopy (AFM). Thermogravimetry-Differential scanning calorimetry (TG-DSC) analysis was conducted by STA 409 PG on 200 mg of the as-deposited film at a heating rate of 10 K/min in static air up to 923 K. Damage testing was performed in the "1-on-1" regime according to ISO standard 11254-1, using 1064 nm Q-switch pulsed laser at a effective pulse duration of 12 ns [12-13]. Damage morphologies after laser radiation were evaluated by a Quanta 250 scanning electron microscope (SEM).

3. Results and discussion

The time dependence of the sol viscosity is given in Fig. 1. The results show that the viscosity increases exponentially with the aging time. During the first 18 days, the viscosity increases slowly, indicating the stability of the sol. The viscosity starts to grow rapidly from the 18th day and it has a remarkable increase from the 32th day. This phenomenon can be explained as below [14]: At the beginning of the aging time, the nucleation in the sol occurs, thus the viscosity increases slowly. Then the particles begin to form larger aggregates, resulting in the accelerated increase of the viscosity. Finally, the aggregates form a three-dimensional network structure and the sol starts to turn into gel, so the viscosity increases remarkably. It is noting that the viscosity increases by only $0.11 \text{ mm}^2 \cdot \text{s}^{-1}$ during 38 days, indicating that the two additives are effective and the sol is very stable.

Fig. 2 shows the transmittance spectra of the films. The transmittance spectra of the film annealed at 423 K keep near the same as that of the film annealed at 353 K, which also remains high transmittance. The transmittance of the films annealed at 523 K and 623 K decreases significantly at the wavelength of more than 500 nm. However, in the range of 420 nm to 500 nm, both these two films still maintain high transmittance. Therefore, the transmittance decrease of the films can be attributed to the thickness change caused by annealing. In addition, the inset picture in Fig. 2 shows that the cut-off wavelengths

have a red shift with the annealing temperature rise due to the band gap decrease [15].

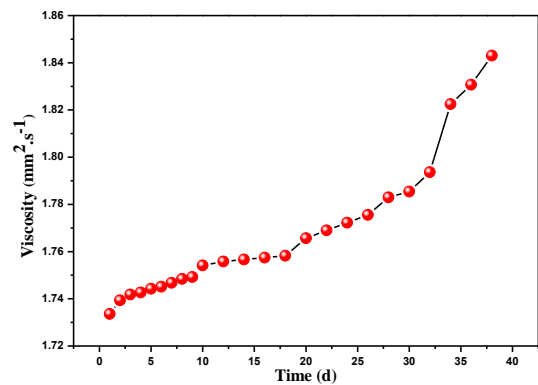


Fig. 1. Time dependence of the sol viscosity

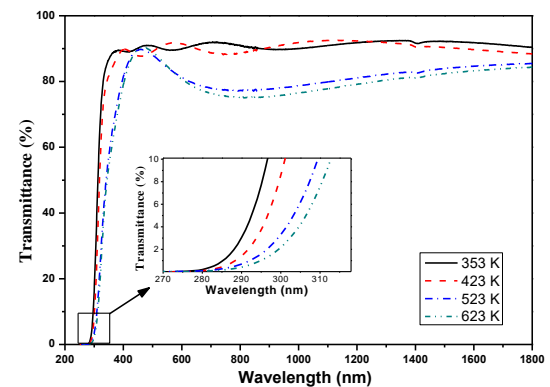


Fig. 2. Transmittance spectra of the films

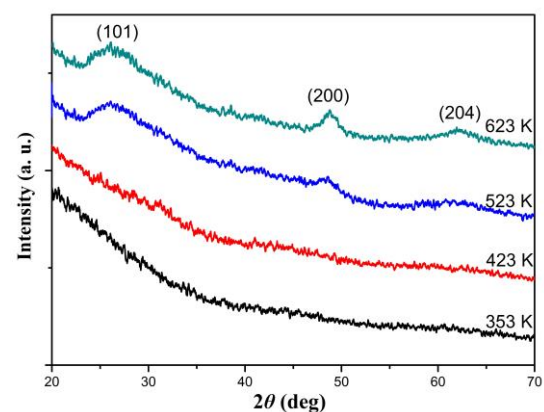


Fig. 3. XRD patterns of the films

The XRD patterns of the films are shown in Fig. 3. It shows that the films remain amorphous when annealed at 353 K and 423 K. However, the film begins to crystallize to anatase phase when annealed at 523 K and the crystalline size grows up with the annealing temperature increase. The average crystalline sizes of the films annealed at 523 K and 623 K are calculated using the Scherrer equation, which are 7.2 nm and 9.6 nm as is shown in Table 1, respectively. It should be noted that the crystal growth will have a negative impact on the LIDT as the grain boundary defects arise.

Table 1 The structure, 2θ , width of half peak β and crystalline size D of the films

Temperature	Structure	2θ (deg)	B (deg)	D (nm)
353 K	amorphous	-	-	-
423 K	amorphous	-	-	-
523 K	anatase	48.49	1.20	7.2
623 K	anatase	48.80	0.893	9.6

Fig. 4 shows the room-temperature photoluminescence spectra of the films. No obvious photoluminescence can be observed for the films annealed at 353 K and 423 K. However, with the temperature increase, both the films annealed at 523 K and 623 K show the photoluminescence bands between 350 nm and 420 nm. This increase of the photoluminescence intensity can be attributed to the gradual growth of TiO₂ nanocrystals with the annealing temperature increase. In addition, with the annealing temperature increase from 523 K to 623 K, the photoluminescence bands shift slightly, indicating the change of the band gap which is in accordance with the transmittance spectra as is shown in Fig. 2.

Fig. 5 shows the FESEM images of the films. No cracking can be found for all the films after annealing. Figs. 5(a) and 5(b) show that both the films annealed at 353 K and 423 K have perfect surface morphologies without defects. However, some large defects as much as 300 nm appear on the surface of the film annealed at 523 K, as shown in Fig. 5(c). When the annealing temperature increases to 623 K, not only large defects appear, but also

many small dot defects emerge on the film surface as is shown in Fig. 5(d), indicating the large increase of the defect density.

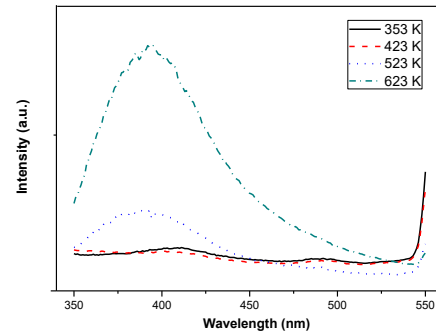


Fig. 4. Photoluminescence spectra of the films

The AFM patterns recorded from the films are shown in Fig. 6. Figs. 6(a) and 6(b) show that the film surface is very uniform and smooth, and the root mean square (RMS) roughness is 0.497 nm and 0.441 nm when annealed at 373 K and 423 K, respectively. Fig. 6(c) shows that the RMS roughness slightly increases to 0.553 nm when annealed at 523 K. It is interesting to note that with the annealing temperature increase to 623 K, some protuberances are found on the film surface, and the surface quality of the film deteriorates, as shown in Fig. 6(d). In addition, the RMS roughness of the film annealed at 623 K increases dramatically to 1.12 nm, which is mainly due to the phase transformation as seen in Fig. 3 and the volatilization of organics in the film at high temperature.

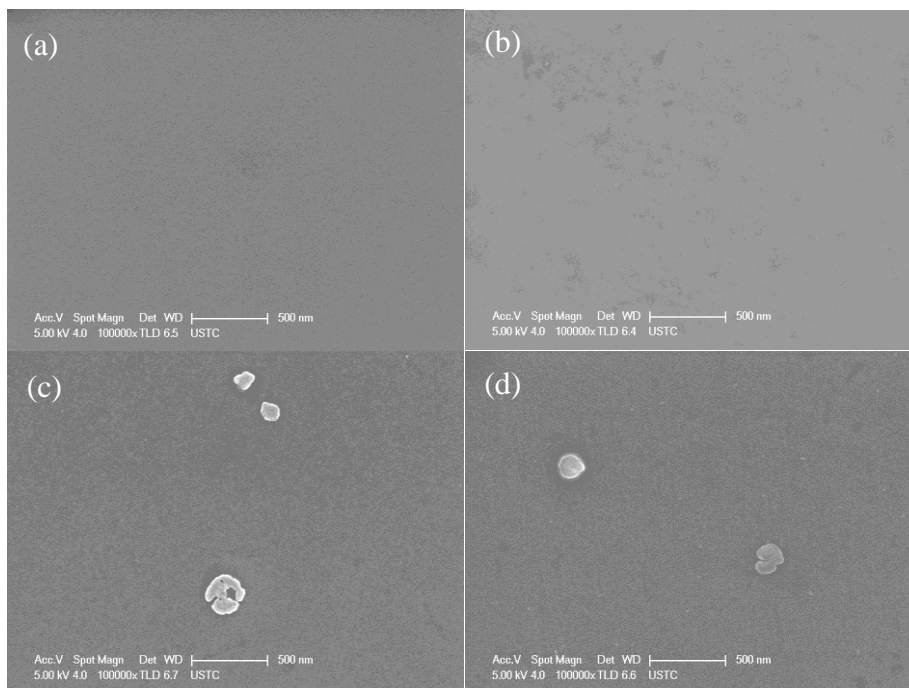


Fig. 5. FESEM images of the films annealed at (a) 353 K, (b) 423 K, (c) 523 K and (d) 623 K

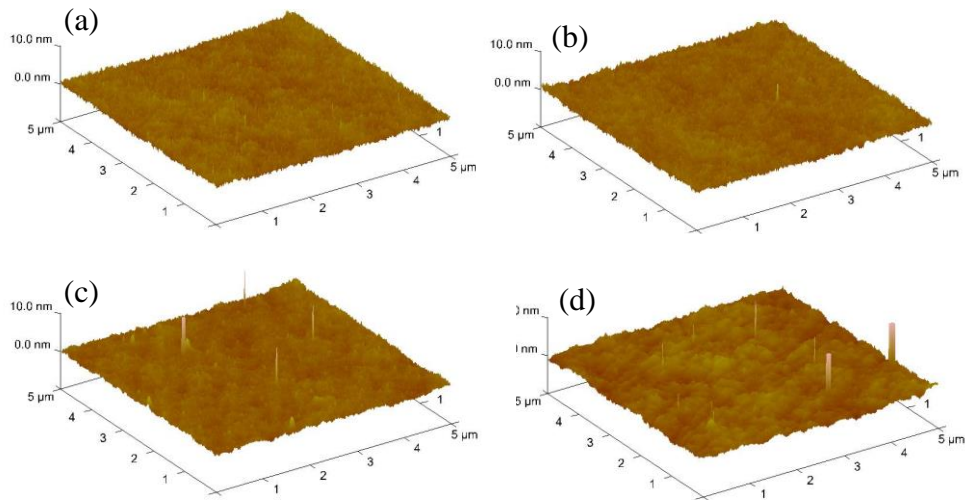


Fig. 6. AFM patterns of the films annealed at (a) 353 K, (b) 423 K, (c) 523 K and (d) 623 K

Fig. 7 illustrates the TG-DSC curves with four stages of the as-deposited film. During the first stage, the temperature rises from 300 K to 373 K alongside with the 2.22% decline of quantity, all of which are attributed to the evaporation of retained water and organics corresponding to the weak endothermic peak in the DSC curve [16]. Then, in the second stage, the temperature increases further up from 374 K to 590 K and the quality decreases by 4.90% correspondingly because of the decomposition of the organics mostly originated from TTIP. There is an exothermic peak in 500 K to 590 K owing to crystallization of TiO_2 . During the third stage, the temperature grows from 591 K to 640 K while the quality goes down sharply by 15.08% mainly due to the evaporation of DEA and PEG 200 counterpart to the endothermic peak in the DSC curve. In the fourth stage, there is a rise in the temperature from 641 K to 923 K and a decline in the quality by 11.09%, which is attributed to the recombination of hydroxy and the decomposition of retained organics.

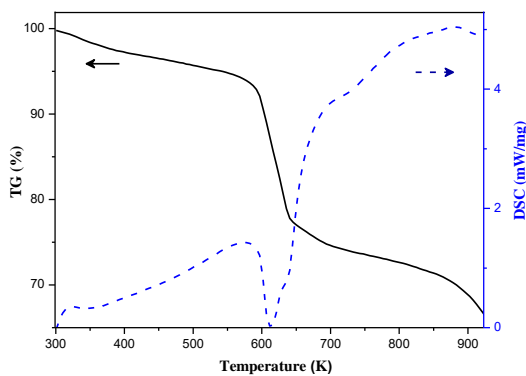


Fig. 7. TG-DSC curves of the as-deposited film

Fig. 8 shows the LIDT results of the films. It shows that the LIDT decreases with the annealing temperature increase. The highest LIDT is 14.3 J/cm^2 obtained by the film annealed at 353 K. When the annealing temperature rises up to 423 K, the LIDT of the film drops by 29.4% to 10.1 J/cm^2 compared to the highest LIDT. However, it is still higher than that of PVD films [17]. With the temperature increasing further to 523 K, the LIDT falls off significantly to 4.0 J/cm^2 with 72.0% down to the highest LIDT. The lowest LIDT is 3.5 J/cm^2 when the film is annealed at 623 K.

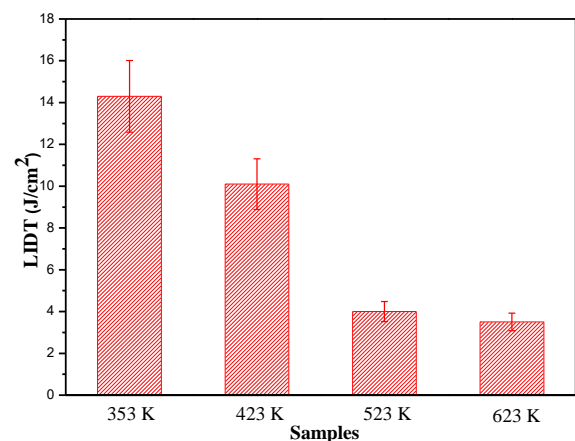


Fig. 8. LIDT results of the films

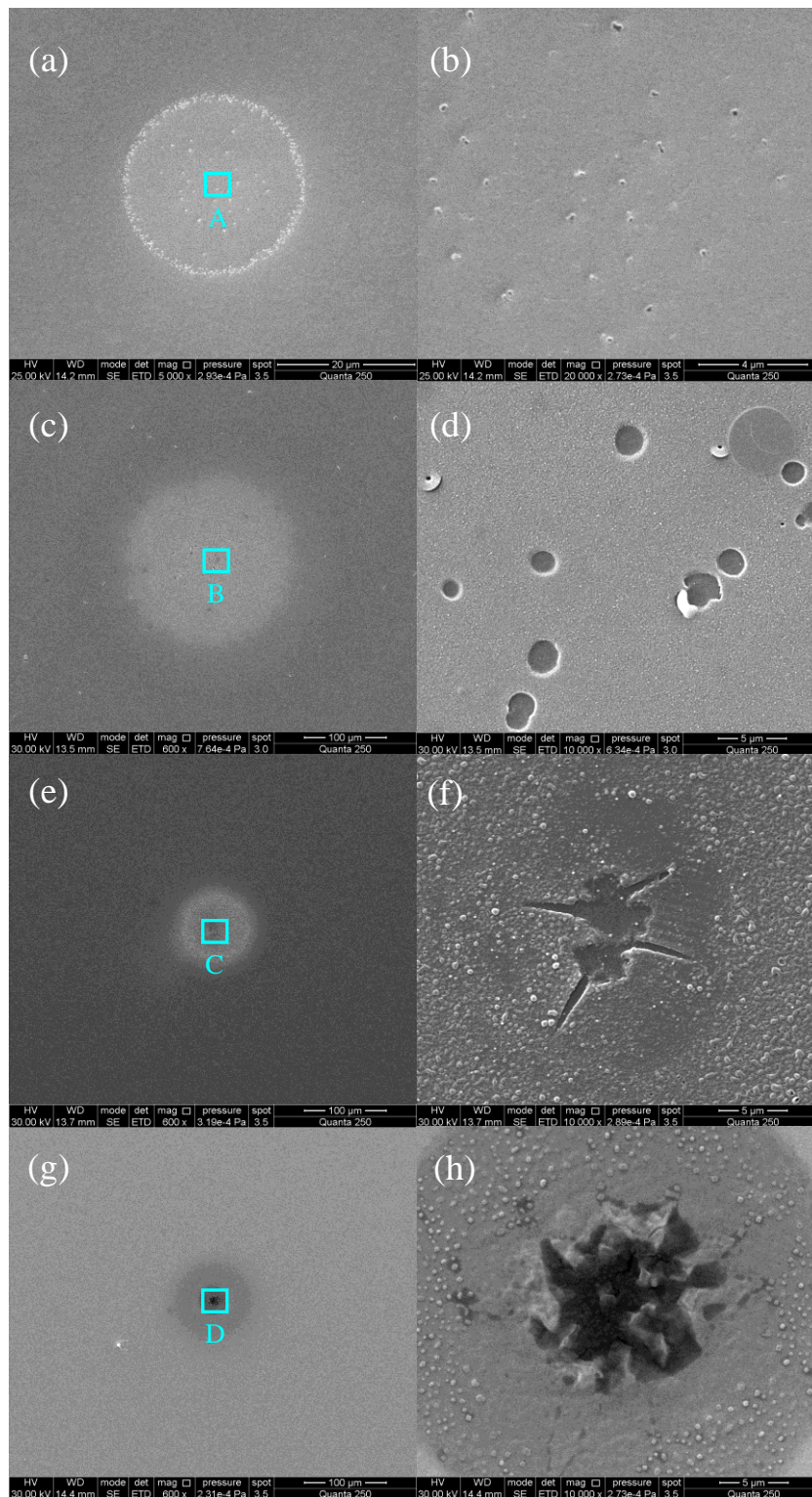


Fig. 9. Damage morphologies of the films annealed at (a) 353 K, (b) enlarged area A, (c) 423 K, (d) enlarged area B, (e) 523 K, (f) enlarged area C, (g) 623 K and (h) enlarged area D

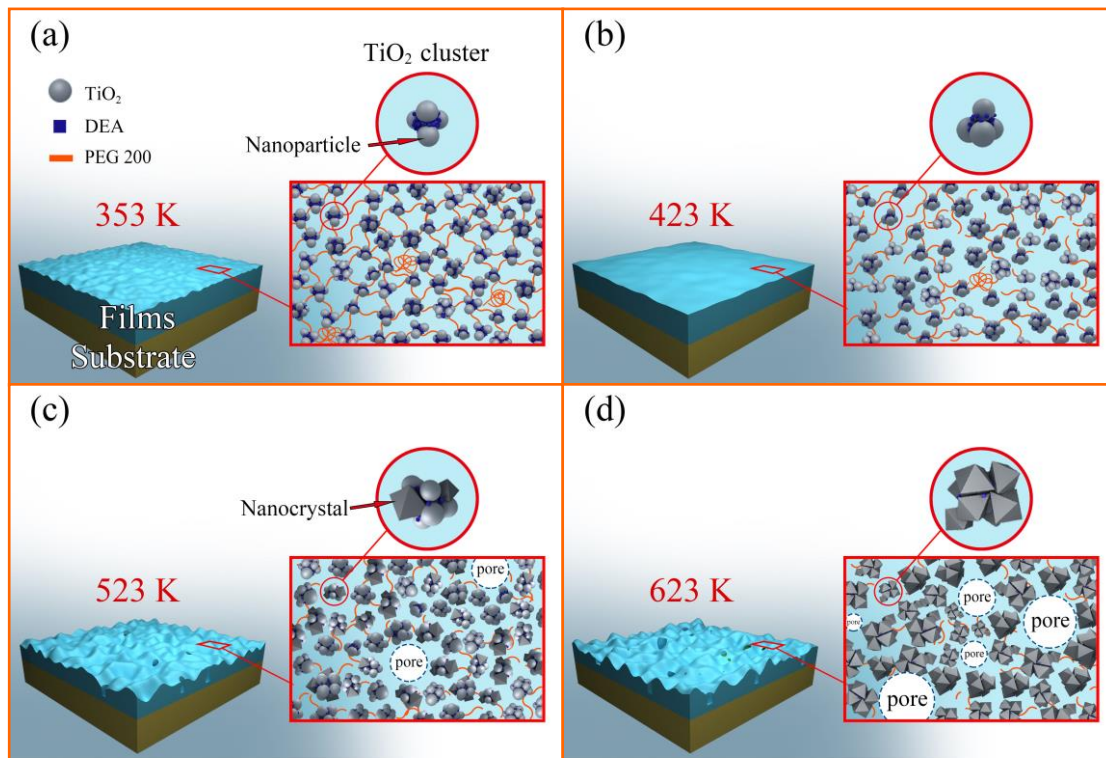


Fig. 10. Structure evolution model of the films at (a) 353 K, (b) 423 K, (c) 523 K and (d) 623 K.

The damage morphologies of the films after laser radiation are shown in Fig. 9. It illustrates that all of these can be ascribed to the defect-induced damage mechanism, the typical characteristic of which is that the damage area has at least one defect [18-19]. The defect has higher absorption coefficient and absorbs more laser energy, so the temperature of the defect rise faster and higher. The film will be damaged once the temperature reaches the melting point or boiling point of the film material [20-21]. In addition, Figs. 9(b), 9(d), 9(f) and 9(h) display that the defect size increases gradually with the annealing temperature increase, which are the enlarged pictures of the four damage areas A, B, C and D in Figs. 9(a), 9(c), 9(e) and 9(g), respectively. Meanwhile, Fig. 9(b) indicates that the damage is initiated by many defects. With the annealing temperature increase, the damage is induced by fewer and fewer defects, as shown in Figs. 9(d) and 9(f). After the highest temperature annealing of 623 K, Figs. 9(g) and 9(h) show that the damage area has only one defect. It is consistent with the FESEM results in Fig. 5 that the defect becomes more and more serious with the annealing temperature increase. An interesting phenomenon is that the damage of the film annealed at 623 K shows different morphology from that of the PVD films and the sol-gel films with single additive [22-24]. The damage center of PVD films after laser radiation shows the circular melting feature, so does the sol-gel films with single additive annealed at more than 523 K. However, both Figs. 9(f) and 9(h) show some organic residues obviously in the damage center. The organics absorb a lot of energy in the laser damage process, reducing the

temperature rise and preventing the total melt of the damage area. After absorbing energy, the organics turn into gases and the volume expands rapidly, resulting in the irregular damage features with cracking and spalling.

4. Discussion

The film annealed at 353 K obtains the highest LIDT of 14.3 J/cm^2 . It is probably mainly due to the three-dimensional network structure and the low defect density of the sol-gel film. The network structure is helpful to relieve the expansion of the film skeleton when absorbing the laser energy, contributing to the LIDT improvement [25-26]. Meanwhile, it has been well recognized that due to its low temperature deposition route, the sol-gel film is free of substoichiometric defects, which is also one of the reasons for the high LIDT. After annealed at 423 K, though the film surface still remains intact without defects and very smooth as is shown in Figs. 5 and 6, the TG-DSC results indicate that some organics are lost from the film. Therefore, the ordered film structure may be damaged to some extent and inner defects emerge. Consequently, the LIDT slightly reduces to 10.1 J/cm^2 . The boiling points of PEG 200 and DEA are 523 K and 542 K, respectively. Therefore, after annealed at 523 K or higher temperature, the organic additives evaporate rapidly. In the meantime, the film starts to crystallize and transform to anatase phase, as shown by XRD results in Fig. 3. Both the additives evaporation and film crystallization lead to the increase of defect density

and surface roughness as is shown in Figs. 5 and 6. Accordingly, the LIDT falls off significantly to 4.0 J/cm² with 72.0% down to that of the film annealed at 353 K. It is worth noting that even after annealing at 623 K, there are still some residual organics in the film according to the damage morphologies in Fig. 9. The possible reason is that the two additives make the evaporation of organics difficult. It will be beneficial for the film to stay intact without cracking at high temperature. Meanwhile, it is well known that the presence of organics earn higher LIDT for the sol-gel films than for the PVD films. Therefore, although the films annealed at higher than 523 K only have very low LIDT in this study, it may provide a possible way to improve the laser damage resistance at high temperature by using two additives in the future.

In addition, base on the LIDT results and damage morphologies, a structure evolution model of TiO₂ films at different temperatures is proposed in Fig. 10. Fig. 10(a) shows the three-dimensional network structure of the film consisting of TiO₂ clusters with similar size assisted by DEA and PEG 200. This film contains maximum amount of organics, and it has the lowest defect density and the highest LIDT. When the temperature increases to 423 K, TiO₂ nanoparticles start to grow up and some organics are lost. Meanwhile, the network structure becomes partially disordered, as shown in Fig. 10(b). It results in the emergence of defects and thereby the decrease of the LIDT. With the temperature climbing up to 523 K, the nanoparticles in the film start to crystallize and transform to nanocrystals. At the same time, the network structure of the film is destroyed seriously due to the large amount of additives evaporation. As a result, the surface roughness of the film increases and a few pores emerge, as shown in Fig. 10(c). Thus, the defect density of the film increases significantly and the LIDT continues to reduce. When the temperature rises further to 623 K, the nanocrystals grow up inhomogeneously. Since only a small amount of organics remain in the film, the network structure is totally destroyed. Consequently, the film surface becomes rougher, and more defects such as the grain boundaries and the holes appear as is shown in Fig. 10(d), resulting in the lowest LIDT.

5. Conclusions

In summary, with the two additives of DEA and PEG 200, a very stable TiO₂ sol is synthesized from TTIP precursor. TiO₂ films are prepared by dip-coating using the sol and remain intact without carbonization and cracking at high temperature. The results show that the nanosecond LIDT decreases with the annealing temperature increase. The highest LIDT is 14.3 J/cm² obtained by the film annealed at 353 K. It is probably mainly due to the three-dimensional network structure and the low defect density. After annealed at 423 K, the ordered film structure is damaged to some extent and inner defects emerge, contributing to the slight reduce of LIDT. With the

temperature increase to 523 K, the additives evaporate rapidly and the film starts to crystallize, resulting in the increase of defect density and surface roughness. Accordingly, the LIDT falls off significantly to 4.0 J/cm² with 72.0% down to that of the film annealed at 353 K. When the temperature rises further to 623 K, only a small amount of organics remain in the film, thus the network structure is totally destroyed. The film surface becomes rougher, and more defects such as the grain boundaries and the holes appear which result in the lowest LIDT. A structure evolution model of TiO₂ films at different temperatures is proposed afterwards.

Acknowledgement

This work is supported by “the Fundamental Research Funds for the Central Universities (2015XKMS065)”, “the Six Talent Peaks Project in Jiangsu Province (2015-XCL-009)” and “Research and Practice on the Teaching Reform of Graduate Education in Jiangsu Province (JGZZ16_080)”.

References

- [1] C. V. Ramana, S. Utsunomiya, R. C. Ewing, U. Becker, V. V. Atuchin, V. Sh. Aliev, V. N. Kruchinin, *Appl. Phys. Lett.* **92**, 011917 (2008).
- [2] C. Xu, D. Li, H. Fan, J. Deng, J. Qi, P. Yi, Y. Qiang, *Thin Solid Films* **580**, 12 (2015).
- [3] C. Xu, M. Ma, H. Sun, D. Lin, P. Feng, J. Qi, Y. Qiang, D. Li, C. Tao, *Optoelectron. Adv. Mat.* **9**, 1337 (2015).
- [4] J. H. Sun, B. H. Wu, H. B. Jia, D. Wu, Y. Xu, *Opt. Lett.* **37**, 4095 (2012).
- [5] Y. Sheng, L. Liang, Y. Xu, D. Wu, Y. Sun, *Opt. Mater.* **30**, 1310 (2008).
- [6] C. Xu, D. Lin, P. Feng, D. Li, H. Fan, J. Qi, J. Niu, Y. Qiang, *J. Optoelectron. Adv. M.* **17**, 1739 (2015).
- [7] Y. J. Guo, X. T. Zu, X. D. Jiang, X. D. Yuan, S. Z. Xu, B. Y. Wang, D. B. Tian, *Opt. Laser Tech.* **40**, 677 (2008).
- [8] C. Xu, P. Yi, H. Fan, J. Qi, S. Yang, Y. Qiang, J. Liu, D. Li, *Preparation Appl. Surf. Sci.* **309**, 194 (2014).
- [9] H. Zhou, D. Yi, Z. Yu, L. Xiao, J. Li, *Thin Solid Films* **515**, 6909 (2007).
- [10] R. S. Sonawane, B. B. Kale, M. K. Dongare, *Mater. Chem. Phys.* **85** 52 (2004).
- [11] H. Li, H. Xiong, Y. Tang, *Chin. Opt. Lett.* **8**, 241 (2010).
- [12] Y. Zhao, Y. Wang, H. Gong, J. Shao, Z. Fan, *Appl. Surf. Sci.* **210**, 353 (2003).
- [13] ISO 11254-1:2000: Lasers and laser-related equipment-determination of laser-induced damage threshold of optical surfaces. Part 1. 1-on-1 test.

- [14] W. Vogelsberger, A. Seidel, T. Breyer, *Langmuir* **18**, 3027 (2002).
- [15] C. Xu, Y. Qiang, Y. Zhu, T. Zhai, L. Guo, Y. Zhao, J. Shao, Z. Fan, *Vacuum* **84**, 1310 (2010).
- [16] J. Park, J. Yun, C. Hwang, I. Lee, *Mater. Lett.* **64**, 2692 (2010).
- [17] J. Yao, J. Shao, H. He, Z. Fan, *Appl. Surf. Sci.* **253**, 8911 (2007).
- [18] J. O. Porteus, S. C. Seitel, *Appl. Opt.* **23**, 3796 (1984).
- [19] S. C. Jones, P. Braunlich, R. T. Casper, X. A. Shen, P. Kelly, *Opt. Eng.* **28**, 1039 (1989).
- [20] S. Papernov, A. W. Schmid, *Appl. Phys.* **97**, 114906 (2005).
- [21] Y. Shan, H. He, Y. Wang, X. Li, D. Li, Y. Zhao, *Opt. Comm.* **284**, 625 (2011).
- [22] C. Xu, J. Jia, D. Yang, H. Fan, Y. Qiang, J. Liu, G. Hu, D. Li, *J. Appl. Phys.* **116**, 053102 (2014).
- [23] Y. J. Guo, X. T. Zu, B. Y. Wang, X. D. Jiang, X. D. Yuan, H. B. Lv, *Optik* **122**, 1140 (2011).
- [24] C. Xu, D. Li, H. Fan, J. Qi, J. Deng, S. Yang, P. Yi, Y. Qiang, *Appl. Sur. Sci.* **344**, 137 (2015).
- [25] F. Chi, L. Yan, H. Lv, C. Wang, X. Yuan, *Thin Solid Films* **519**, 2483 (2011).
- [26] X. Li, M. Gross, B. Oreb, J. Shen, *J. Phys. Chem. C* **116**, 18367 (2012).

*Corresponding author: xucheng@cumt.edu.cn